Tampau, A.; González Martínez, MC.; Chiralt, A. (2018). Release kinetics and antimicrobial properties of carvacrol encapsulated in electrospun poly-(epsilon-caprolactone) nanofibres. Application in starch multilayer films. Food Hydrocolloids. 79:158-169. doi:10.1016/j.foodhyd.2017.12.021

Release kinetics and antimicrobial properties of carvacrol encapsulated in electrospun poly-(ε-caprolactone) nanofibres. Application in starch multilayer films.

Alina Tampau [a,1,*], **Chelo González-Martínez** [b,2], **Amparo Chiralt** [c,3]

[a, b, c] Instituto Universitario de Ingeniería de Alimentos para el Desarrollo, Ciudad Politécnica de la Innovación, Universitat Politécnica de Valencia, Camino de Vera, s/n, 46022 Valencia, Spain.
[1] altam@upv.es, [2] cgonza@tal.upv.es, [3] dchiralt@tal.upv.es

Abstract

Electrospun poly-(ε-caprolactone) (PCL) fibre mats encapsulating Carvacrol (CA) were obtained with good encapsulation efficiency (85%) and CA load (11 % in the fibre). These mats were effective at controlling the growth of *Escherichia coli*, when the surface density of CA loaded fibres was 1.2 or 1.8 mg/cm^2, in line with the CA released into the culture medium that exceeded the MIC of the bacteria. However, they were not effective at controlling the growth of *Listeria innocua*, since a greater release of CA was necessary to achieve the MIC of this bacterium. It was not only the CA load in the fibres, but also its release capacity in the media that determined the antimicrobial effect. The fibre showed higher release rate and ratio in less polar simulants, D1 (50% ethanol) and D2 (isooctane) (representing fatty foodstuff), where practically the total amount of CA was released; whereas in more polar systems (simulants A (10% ethanol) and B (3% acetic acid)) a more limited CA delivery (60-75 %) occurred, at a slower rate. The antimicrobial action of the active PCL mats was reproduced in multilayer starch films containing the CA-loaded electrospun PCL fibres between two starch sheets, with a slightly delayed response. In the multilayer films, a great reduction in the water vapour permeability was also observed with respect to that of starch films, without relevant changes in other functional properties of the films for packaging purposes.

Keywords: PCL, carvacrol, release kinetics, antimicrobial action, starch multilayer films

1. Introduction

The electrohydrodynamic process known as electrospinning is an efficient and straightforward method with a simple working principle (Bhardwaj & Kundu, 2010) that allows micro- and nanoscale polymer structures to be obtained. It can generate continuous (fibres) or discrete (particles) polymer delivery systems able to encapsulate compounds of specific interest for applications in many fields, such as that of medicine (Hamori et al., 2014; Sill & von Recum, 2008), optoelectronics (Hernández-Martínez, Nicho, Hu, León-Silva & Arenas-Arrocena, 2017; Xue et al, 2017), sensor technology (Mercante, Scagion, Migliorini, Mattoso & Correa, 2017;

* Corresponding author. E-mail address: altam@upv.es (Alina Tampau).

Macagnano & De Cesare, 2017) or food packaging (Fabra, López-Rubio & Lagaron, 2016). Incorporating active natural compounds into biodegradable food packaging materials is an innovative trend that focuses on the enhancement of the quality and shelf-life lengthening of the packaged foods (Majid, Nayik, Dar & Nanda, 2016; Padgett & Han, 1998), while these biodegradable materials reduce the environmental impact of the packaging waste. The electrospinning technique could be a feasible way to encapsulate the active compound, while providing a controlled delivery system (electrospun layer) when applied to such packaging materials. Electrospun layers provide structures with a large specific surface area for the compound diffusion, while the losses of active compounds during the process are minimized due to the use of room temperatures.

Of the active agents that are currently used in the development of active food packaging, plant essential oils (and their constituents) are a prominent group of interest. Plant-derived phenolic terpenoids have been successfully incorporated in different polymers with food packaging potential, as reported by Requena, Vargas & Chiralt, (2017) for eugenol encapsulated in poly(hydroxybutyrate-co-hydroxyvalerate), Fernandez-Pan, Maté, Gardrat & Coma, (2015) for carvacrol in chitosan, Rieger & Schiffman, (2014) for cinnamaldehyde in chitosan/poly(ethylene-oxide) or Ramos, Beltrán, Peltzer, Valente & Garrigós, (2014) for carvacrol and thymol in polypropylene. Carvacrol is one of the most widely used active compounds (Higueras, López- Carballo, Hernández-Muñoz, Catalá & Gavara, 2014) recognized as a food additive (Joint FAO/WHO, 2001) and as a flavouring substance (EFSA, 2012). It is a phenolic terpenoid present at great concentration in several essential oils, such as oregano or thyme oil (Burt, 2004), which exhibits high antimicrobial activity against both Gram positive and Gram negative bacteria (Ben Arfa, Combes, Preziosi-Belloy, Gontard & Chalier, 2006; Ultee, Gorris & Smid, 1998), as well as different fungi (Tunc, Chollet, Chalier, Preziosi-Belloy & Gontard, 2007). Its incorporation in food-grade polymers would offer alternative active packaging materials, replacing some of the synthetic antimicrobials currently in use such as weak organic acids or salts (Fu, Sarkar, Bhunia & Yao, 2016). Its controlled delivery, until the minimal inhibitory concentration of the microorganisms is reached at the target point, is required to ensure its antimicrobial activity. This controlled release should also prevent any overdose in the food system in order to limit the dilution effects by diffusion and the food sensory impact.

A previous study (Tampau, González-Martínez & Chiralt, 2017) reported a good encapsulation efficiency (EE) of carvacrol in electrospun poly-ε-caprolactone (PCL) mats, using 15 % glacial acetic acid solution of PCL containing 0.15 g carvacrol / g polymer. These mats exhibited a fibrous structure, which could adequately coat biodegradable packaging films to obtain active materials for food applications. 85% of the carvacrol content of the solution could be encapsulated in the PCL fibres, which is highly efficient when taking into account the volatile nature of the active and the high losses incurred by other techniques. Despite the high EE, the

antimicrobial effect of the encapsulated compound will be affected by its initial load in the active material and its active release capacity into the applied medium. All of this defines the active effective concentration on the target point, which must exceed the minimal inhibitory concentration of the contaminating bacteria.

Likewise, electrospun PCL fibres carrying carvacrol could be applied to obtain multilayer starch films including carvacrol loaded fibres between the starch sheets, thus contributing to the improvement of the functional properties of the packaging material. The multilayer assembly of biopolymers with complementary properties allows packaging material to be obtained that better meets the specific requirements of different kinds of foods. In fact, more and more of the food available in the stores comes in high-tech plastic packaging multilayer films, ensuring the food is preserved for longer than when using a monolayer structure. Starch is a good candidate since it is widely available and cheap, while its films are extensible with very good oxygen barrier properties (López, Zaritzky, Grossmann, & García, 2013). However, starch films exhibit poor water vapour barrier capacity, being water sensitive (Pushpadass et al., 2009). In this sense, PCL exhibits good barrier capacity to water vapour (Ortega-Toro, Morey, Talens & Chiralt, 2015) and its inclusion in the starch multilayer assembly has been demonstrated to enhance the film functionality (Ortega-Toro et al., 2015). Likewise, the incorporation of carvacrol into the PCL electrospun layer can confer antimicrobial properties on the starch/PCL/starch multilayers.

The aim of the study was to develop active electrospun layers of poly-ε-caprolactone with encapsulated carvacrol with a high enough load of the active to be applied on food packaging films, by analysing the release kinetics of carvacrol in different food simulants (solvents with different polarity) and verifying their antibacterial activity. Likewise, the improvement in the functional properties of the starch multilayer films, containing electrospun PCL fibres between the starch sheets, has been analysed in terms of the barrier and tensile properties and antimicrobial activity.

2. Materials and methods

2.1. Materials and reagents

Poly-(ε-caprolactone) (PCL) pellets (average Mn 80,000) and carvacrol (CA) were acquired from Sigma-Aldrich (Sigma–Aldrich Chemie, Steinheim, Germany). All UV-grade solvents used (ethanol, glacial acetic acid and isooctane) were from Panreac AppliChem (Panreac Química S.L.U, Barcelona, Spain).

2.2. Obtaining and characterizing the electrospun fibre of CA-loaded PCL

On the basis of previous studies (Tampau et al., 2017), nanofibres were obtained from PCL in glacial acetic acid (GAA) with and without CA. Briefly, PCL (15 wt %) and CA (15 wt % with respect to the polymer) were dissolved in GAA under stirring for 24 h at room temperature. The solutions were electrospun using Fluidnatek equipment (BioInicia S.L., Valencia, Spain), at a

flow rate of 1.2 mL/h through the syringe needle (internal diameter=0.6 mm), by applying an electric field of 12.0 kV. The electrospun fibre material was collected on aluminium foil disks placed on the collector at 20 cm from the tip of the needle. In these conditions, an encapsulation efficiency (EE) of CA in the fibres of about 85 % was expected, which would suppose 12 g CA/100 g fibres in the obtained mat.

Nanofibres were obtained for different electrospinning (ES) times on aluminium foil to determine the process yield (g fibre/cm^2) as a function of the process time. Carvacrol content in the fibre (mg/g fibre) was analysed at the longest process time (90 min) and the expected EE from the previous study (Tampau et al. 2017) was verified. The CA surface density (mg CA/cm^2) vs the ES time was estimated from this analysis, in order to determine the time required to reach enough CA load in the mat. This is for the purposes of ensuring that the minimum inhibitory concentration (MIC) of CA for different bacteria can be reached when the active mat is applied on a target product surface. Likewise, CA content was also determined in different zones of the circular electrospun surface, considering radial distance and angle with respect to the centre (6 zones), to analyse the CA distribution homogeneity on the mat surface electrospun for 90 min.

CA quantification was carried out by extraction of fibre (with a determined surface and weight) with UV grade absolute ethanol and spectrophotometric determination at 275 nm using a UV/Vis spectrophotometer (Evolution 201 UV-Vis, Thermo Fisher Scientific Inc.), as previously described by Tampau et al. (2017). The obtained results were expressed as μg CA/cm^2 or μg CA/g fibre.

Structural characterization of the fibres was performed using Field Emission Scanning Electron Microscopy (FESEM Ultra 55, Zeiss, Germany). Samples were mounted on support stubs and, after platinum coating, were observed using an accelerating voltage of 2 kV. ImageJ software (National Institutes of Health, U.S.A.) was employed for the image analysis, in order to assess the morphological differences between the two types of matrices with or without the active.

2.3. Release kinetics of CA in different food simulants

The kinetic study of CA release from the electrospun PCL fibres was carried out in four types of solvents, acting as food simulants of different polarities or pH (Regulation 10/2011/EC). As described by Requena et al. (2017), ethanol 10% (v/v) (simulant A) and acetic acid 3% (w/v) (simulant B) were chosen to emulate aqueous foodstuffs neutral and acidic (pH<4.5) in character, respectively. Ethanol 50% (v/v) (simulant D1) was used to imitate foods with alcohol content higher than 20% or oil-in-water emulsions, whereas isooctane (simulant D2) was used for foods with a highly lipophilic surface. For this purpose, fibre samples of 50 mg were placed in glass bottles containing 100 mL of the corresponding simulant, and kept under stirring at 22 ± 2 ºC. Aliquots of the samples were extracted at different times of contact (ranging from 1 min upward, until equilibrium is reached) and absorbance was determined spectrophotometrically at

275 nm. CA quantification in the liquid phase was established using the previously obtained calibration curves in each simulant. All analyses were carried out in triplicate, using the respective simulant, in contact with CA-free fibres for the equivalent time, as blank.

2.3.1 CA release mathematical modelling

Three models were considered to describe the behaviour of the CA loaded PCL fibres in the four food simulants. Considering that the electrospun fibres fuse together at different points throughout their length to form a mat-like matrix, the CA release from the mat can be analysed as a one-dimensional mass transfer process from an infinite plane sheet (Crank, 1975) of half-thickness *e*, with a characteristic diffusion coefficient D (m^2/s). The diffusion coefficients for each simulant were determined by modelling the obtained data to Fick's second law for long-time diffusion (eq.1), considering that i) the distribution of the active is homogenous within the matrix, ii) the initial concentration of CA in each simulant is zero, and iii) there is no degradation of CA during the migration process.

$$\frac{M_t}{M_\infty} = \frac{8}{\pi^2}\sum_{n=0}^{\infty}\left[\frac{1}{(2n+1)^2} exp\left\{\frac{-D(2n+1)^2\pi^2 t}{4e^2}\right\}\right] \text{(eq. 1)}$$

where:

t = release process time (s),

M_t = mass of CA released at time t,

M_∞ = mass of CA released at equilibrium,

e: half thickness of the fibre layer (m).

The boundary conditions taken into account for eq.1 are as follows:

$$t = 0 \qquad -e < x < e \qquad c = c_0$$

$$t > 0 \qquad x = \pm e \qquad c = 0$$

The mathematical solutions from Fick's equation with eleven terms **(n= 0÷10)** were optimized using the Solver tool (Microsoft Excel 2016®) by minimizing the Sum of Squared Errors **(SSE).**

Peleg's model (eq. 2) (Peleg, 1988) was also applied to the data, in order to obtain the equilibrium value for the carvacrol release and the release rate for each simulant.

$$\frac{t}{M_t} = k_1 + k_2 t \quad \text{(eq. 2)}$$

where:

t = release process time,

175 M_t = mass of CA released at time t,

176 $1/k_1$ = release rate,

177 $1/k_2$ = mass of CA released at equilibrium (M_∞).

178 Lastly, the Korsmeyer-Peppas model (Siepmann & Peppas, 2011) (eq. 3) was considered in
179 order to analyse the mechanisms controlling the CA release, with the caveat that it can only be
180 applied for ($\frac{M_t}{M_\infty} \leq 0.6$), which means a progress of the mass transfer process of 60% (Hines &
181 Kaplan, 2011).

182

183 $$\frac{M_t}{M_\infty} = kt^n \quad \text{(eq. 3)}$$

184 where:

185 M_t/M_∞= mass of CA released at time t with respect to the mass released at equilibrium;

186 t = release process time (h);

187 k = rate constant (h^{-n});

188 n = diffusional exponent which takes values in the 0÷1 interval (dimensionless).

189 **2.3.2. Prediction of CA antimicrobial effect based on the release study**

190 Peleg's parameters determined in the modelling step were employed to predict the amount of
191 CA released throughout time in the target product, which must reach the minimum inhibitory
192 concentration (MIC) of the target microorganism to exert the antimicrobial effect. To this end, a
193 contact surface equivalent to a Petri dish of 5.5 cm in diameter with a volume of 10 mL of agar
194 medium (pH=5.6±0.2) was considered. For this simulation, two ES deposition times of 60 and
195 90 minutes (with the subsequent total amount of CA in the mat) and the release profile of CA
196 from PCL mats in A simulant were considered. Simulant A was the most similar in water
197 content to the culture medium.

198 **2.4. Incorporation of PCL fibres in multilayer starch films**

199 PCL fibres were electrodeposited on thermoplastic starch films (S) in order to obtain multilayer
200 films (S-PCL-S). To this end, corn starch films were obtained by melt blending of starch-
201 glycerol-water (mass ratios: 100:30:50) at 160ºC and 8 rpm for 30 min in a two-roll mill (Model
202 LRM-M-100, Labtech Engineering, Thailand). The obtained pellets were conditioned at 53%
203 relative humidity for 1 week and compression moulded in a press (Model LP20, Labtech
204 Engineering, Thailand), initially at 50 bars/160 ºC for 2 min, then at 130 bars/160 ºC for 6 min,
205 and cooled down to 50 ºC for 3 min (Ortega-Toro et al., 2015). Multilayer films were prepared
206 by electrodeposition of the 15 % PCL solution in GAA with or without CA (15 g/100 g PCL).
207 Electrodeposition times were 60 and 90 min to obtain the same CA surface concentration as in
208 previously described fibre mats. Multilayer films with the ES PCL in the middle were obtained

by thermocompression of two S layers (one of these containing the ES PCL fibres of 60 or 90 min) at 130 bars and 80 ºC for 4 min, and cooled down to 50 ºC for 2 min.

Multilayer films conditioned for 1 week at 53 % RH were characterized as to their thickness (measured at 5 different points by a Palmer digital micrometre from Comecta, Barcelona, Spain), water content (assessed gravimetrically), water vapour permeability (determined at 25 ºC using a modified (Gennadios, Weller & Gooding, 1994) ASTM E96-95 gravimetric method (ASTM, 1995), as described by Perdones, Chiralt & Vargas, (2016)), oxygen permeability (Standard Method D3985-95 (ASTM, 2002)) and tensile properties (ASTM standard method D882 (ASTM, 2001)), as previously described by Ortega-Toro et al. (2015).

Antimicrobial *in vitro* tests were also carried out for multilayer films using the below described method (section 2.6) for fibre mats.

2.5. Thermal analysis

Thermal analyses were carried out in PCL fibres and multilayer assemblies in order to analyse the carvacrol effect on phase transitions and thermal stability of PCL or starch. Differential scanning calorimetry analyses were performed, using a DSC (1 StareSystem, Mettler-Toledo, Inc., Switzerland). Samples (5-15 mg), previously conditioned in P_2O_5, were placed into aluminium pans (Seiko Instruments, P/N SSC000C008) and sealed. Samples were heated from 25ºC to 120 °C at 10 K/min. Then, they were kept at 120 °C for 5 min, cooled to -60 °C at -10 K/min, kept at -60 °C for 5 min and heated again to 200 °C at 10 K/min. An empty aluminium pan was used as reference. Each sample was analysed in triplicate.

A thermo-gravimetric analyser (TGA/SDTA 851e, Mettler Toledo, Schwarzenbach, Switzerland) was used to characterize the sample thermal degradation. The analysis was performed from room temperature to 500 °C at 20 °C/min under a nitrogen flow (50 mL/min). DTA and DGTA curves were analysed and the temperature at which the maximum degradation rate occurs was determined (T_{max}). Each sample was analysed in duplicate.

2.6. Antimicrobial properties

Gram (+) *Escherichia coli* (CECT 101) and Gram (-) *Listeria innocua* (CECT 910) obtained from Spanish Type Culture Collection (CECT, Burjassot, Spain) were used to test the antimicrobial efficiency of the electrospun PCL fibre mats. The model bacterial strains, stored in protective conditions (glycerol 30%) at -25 ºC, were regenerated as described by Valencia-Sullca et al. (2016), by incubating them at 37 ºC for 24 h in tryptic soy broth (TSB) (Scharlab, S.L., Barcelona, Spain) and harvested in their exponential growth phase. The revived cultures were properly diluted in TSB to obtain a target inoculum of 10^6 colony forming units (CFU)/ml for *E. coli* and 10^5 CFU/ml for *L. innocua*.

Circular samples (55 mm in diameter), consisting of starch multilayers or PCL fibre mats (with and without CA) electrospun over thermoplastic starch film acting as support, were placed (with

the electrospun side face down) on inoculated plates (1 ml inoculum on the plate surface) containing 10 mL of tryptic soy agar (TSA) (Scharlab, S.L., Barcelona, Spain). CA-free PCL samples and uncoated inoculated TSA plates were used as controls. Immediately after the inoculation and after 2, 6, 9 and 14 days of storage at 10 ºC, microbial counts were performed. To this end, the Petri dish content was placed aseptically in a sterile stomacher strainer bag (Seward Limited, West Sussex, UK) along with 90 mL of buffered peptone water (BPW) (Scharlab, S.L., Barcelona, Spain) and homogenized for 2 min by means of a Masticator Paddle Blender (IUL S.A., Barcelona, Spain). Serial dilutions of this liquid were plated and covered with violet red bile agar (VRBA) (Scharlab, S.L., Barcelona, Spain) for *E. coli* and palcam agar base (PAB) (Scharlab, S.L., Barcelona, Spain) enriched with palcam selective supplement for *Listeria* (Scharlab, S.L., Barcelona, Spain). After incubation at 37 ºC for 48 h, the colonies were counted. All determinations were performed in duplicate.

2.7. Statistical analysis

The experimental data was processed using one-way analysis of variance (ANOVA) with the statistics program Statgraphics centurion XVI.I (StatPoint Technologies Inc. Warrenton, VA, USA).

3.Results and discussion

3.1. Electrospun fibre layers of CA loaded PCL

The structure of the obtained electrospun matrices can be observed in Figure 1. The mat has a fibrous appearance, with occasional beads of spindle-like geometry which appear more frequently in the case of the CA-loaded fibres. The average diameter of active-loaded fibres was 200±40 nm, whereas in the case of the CA-free matrix this reached higher values of 500±350 nm. CA affected the morphology of the electrospun fibres, giving rise to thinner fibrous forms, but with more beads, such as previously observed (Tampau et al., 2017). These changes must be attributed to the differences in the liquid phase properties induced by CA addition and the CA interactions with the polymer chains that affected the chain entanglements, responsible for fibre formation (Bahrami & Gholipour Kanani, 2011).

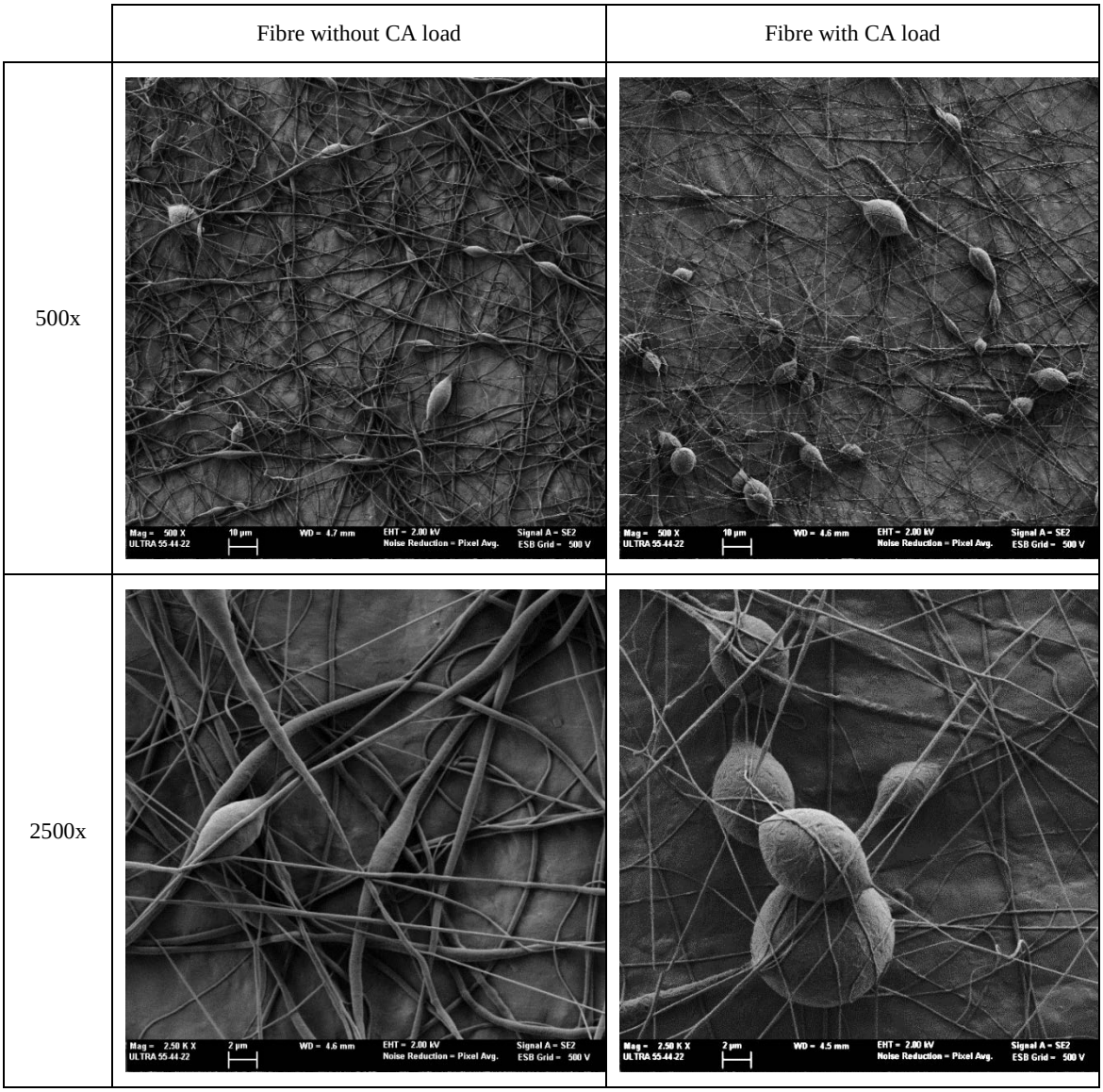

Figure 1. FESEM micrographs of the electrospun fibres for 10 minutes.

The mass fibre accumulation on the collector surface as a function of the ES time (Figure 2a) reveals the expected linear trend where the slope is coherent with the liquid flow applied in the equipment, the concentration of the compounds (PCL and CA) and the EE of CA. The quantified amount of CA in the fibre obtained for 90 min was 11.1±0.1 g CA/100g fibre. This concentration represents an encapsulation efficiency of CA in the fibres of 83±1% (expressed as the ratio between the final amount in the fibre and the initial content in the solution), which agrees with the values previously reported by Tampau et al. (2017). From the mean CA content in the fibre, the CA surface density in the ES layer as a function of time was predicted (Figure 2b). Figure 2b also shows the values of the minimal inhibitory concentration (MIC) reported by some authors for *Escherichia coli* and *Listeria monocytogenes*, expressed as $\mu g/cm^2$. To obtain these values, the reported MIC values of CA against *E. coli* ($2.2 \cdot 10^{-4}$ g/ml) and *L. monocytogenes* ($3.7 \cdot 10^{-4}$ g/ml) (Burt, 2004), and the *in vitro* test conditions for the antimicrobial

activity of the fibres used in the present study (section 2.4), were considered. Then, the MIC (μg/ml) was assumed to be reached in 10 ml of medium with a contact surface of 23.76 cm^2 (in a plate of 5.5 cm diameter) with the fibre mat. Figure 2b is a useful tool with which to estimate the ES time required to obtain active electrospun layers of PLC-CA fibres with enough CA to exceed the MIC of different microorganisms.

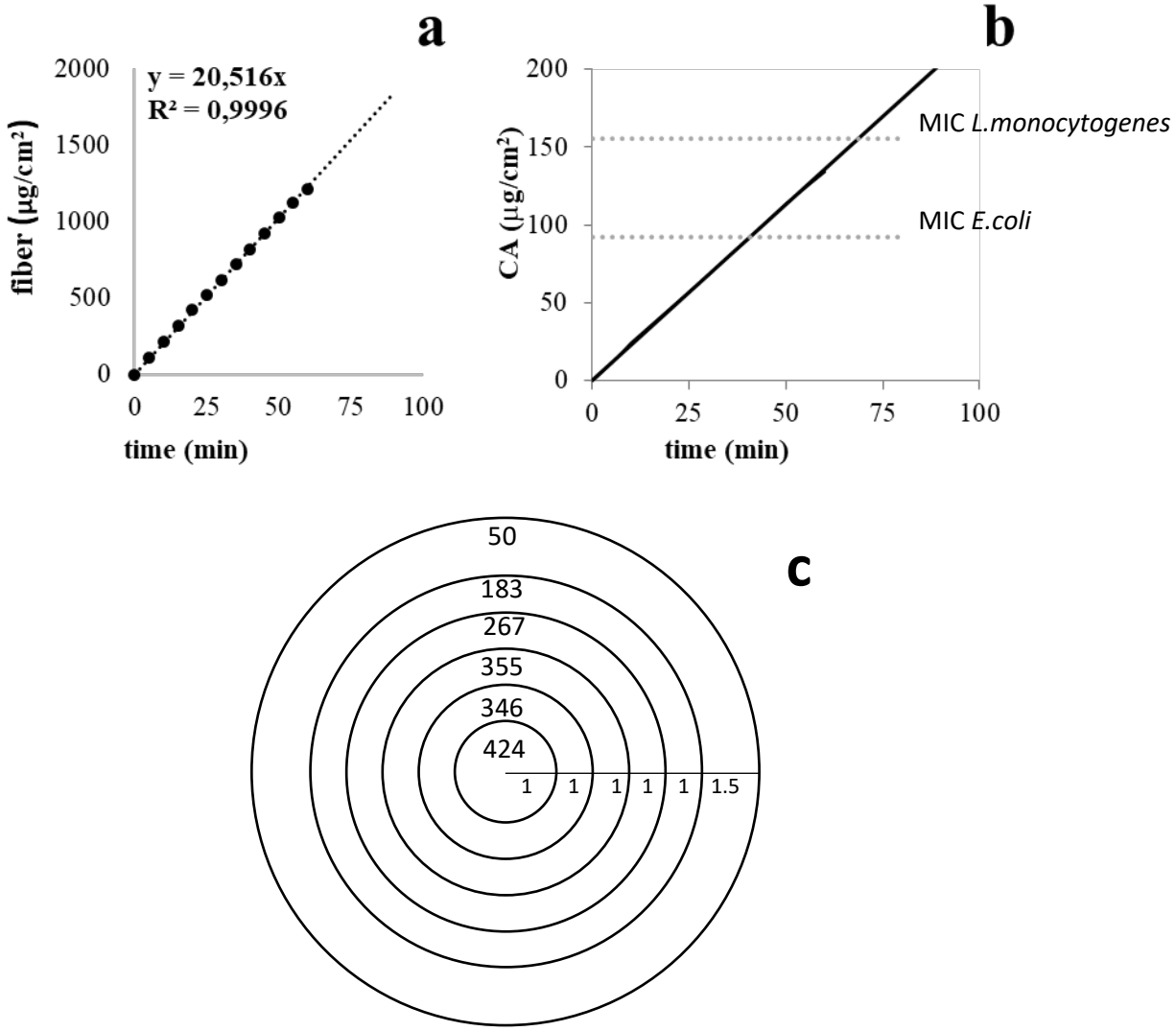

Figure 2. **a)** Mass of ES fibre layer as a function of time; **b)** Mean surface density of CA (μg/cm^2) as a function of ES time and **c)** surface CA distribution (μg/cm^2 in different zones of ES layer) for 90 min of ES (radius increments shown in cm). MICs in μg/cm^2 are indicated as a dashed line, assuming a CA diffusion in 10 ml medium through 23.76 cm^2 of sample surface in contact with the fibres (equivalent to 0.42 cm of characteristic dimension for diffusion).

An ES time of 37 min and 62 min, respectively, would be required to obtain a CA mass in the fibres equivalent to the respective MICs of each bacterium. In order to ensure this quantity of active is reached, 60 and 90 min of ES time were applied to obtain potentially active layers, assuming that the complete release of the active in the culture media could not occur. By analysing the active's surface distribution, additional data was obtained to support this decision; this revealed that the ES process with the used equipment provided an uneven coating, creating

a concentric concentration gradient (Figure 2c), where the external area of the obtained electrospun disc contained a smaller amount of fibres and so of CA. In this sense, four tangent sample disks obtained from each of the four quadrants of the main circle were considered for each analysis.

3.2. Release kinetics of CA from PCL fibres in different food simulants

The release kinetics of CA from the fibre mat obtained for 90 min was analysed in order to find out how the active compound can be delivered in different food systems. To this end, four liquid simulants of different polarity have been considered, as commented in section 2.3. The release mass of CA was determined at different contact times with simulants and Figures 3 and 4 show the mean values, for each food simulant.

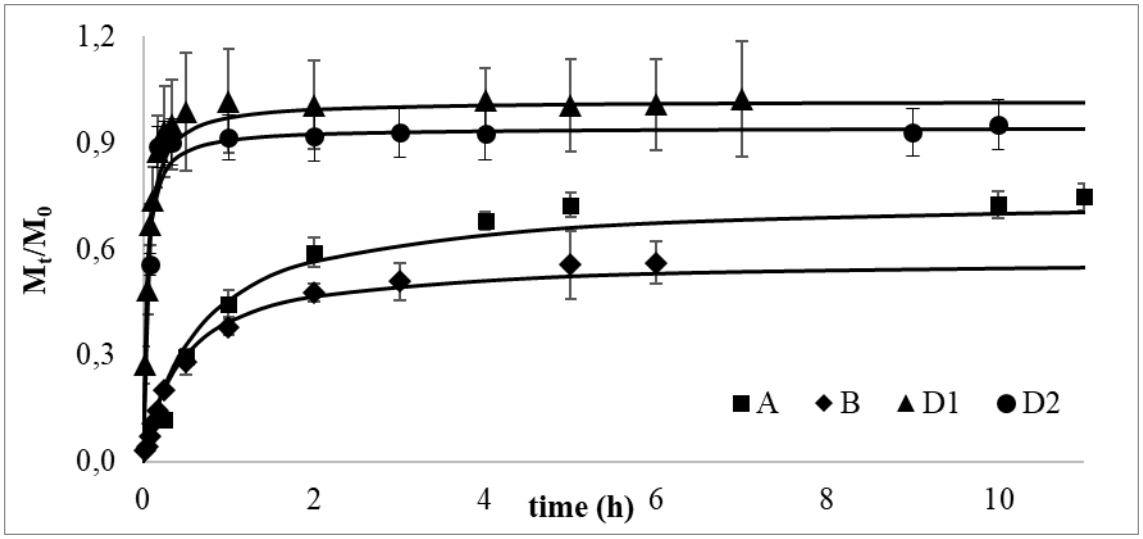

Figure 3. M_t/M_0 ratio (fraction of the active released from the fibres at each time, referred to the initial content in the fibres) as a function of time for the different solvents: experimental data (points) and Peleg's fitted model (continuous lines).

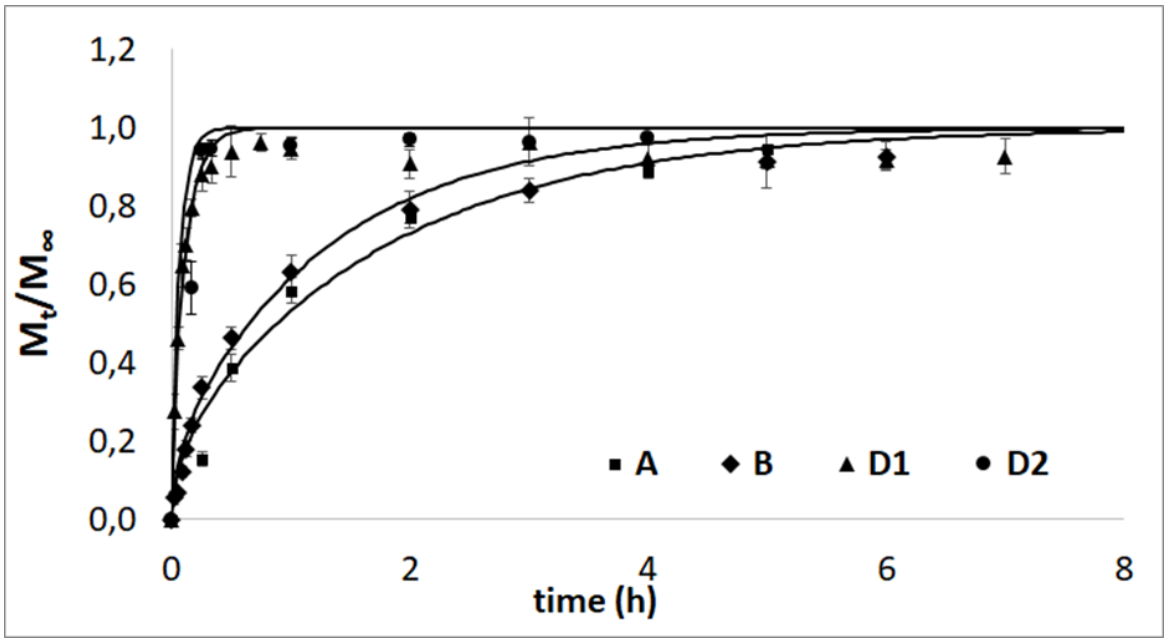

Figure 4. M_t/M_∞ ratio (fraction of the active released from the fibres at each time, referred to the maximum value released at equilibrium) as a function of time for the different simulants: experimental data (points) and Fick's fitted model (continuous lines).

Table 1. Parameters of the Peleg ($\mathbf{M_\infty}$ - CA mass released at equilibrium; $\mathbf{1/k_1}$ - CA release rate) and Korsmeyer-Peppas (**n** - diffusional exponent; **k** - rate constant) models, and Fick's diffusion coefficient in the different food simulants. The $\mathbf{M_\infty/M_0}$ ratio represents the CA mass released in the simulant liquid at equilibrium, with respect to the total amount in the fibres determined by ethanol extraction. Different superscript letters in the same column indicate significant differences ($p<0.05$) between simulants.

	Adjusted model								
	Peleg				**Fick**		**Korsmeyer-Peppas**		
Simulant	**$1/k_1$ (μg CA/g film)**	**$M_\infty=1/k_2$ (g CA/100 g film)***	**M_∞/M_0 (%)**	**R^2**	**$Dx10^{13}$ (m^2/s)**	**SSE**	**n**	**K (h^{-n})**	**R^2**
A	34,1±0,4^a	7,8±0,3^b	75±3^b	0,9993	3,9±0,3^a	0.03	0,9±0,2^c	0,63±0,05^a	0,9468
B	38±2^a	6,1±0,6^a	57±5^a	0,9998	5.3±1^a	0.12	0,68±0,04^b	0,67±0,01^a	0,9502
D1	700±150^b	11±1^c	100±10^c	0,9981	46±7^b	0.04	0,53±0,07^{ab}	2,3±0,3^c	0,9979
D2	800±100^b	11,5±0,8^c	96±7^c	0,9998	109±14^c	0.05	0,46±0,11^a	1,8±0,4^b	0,8747

***corresponding to 100 mL volume of simulant

Table 1 shows the maximum values released (M_∞), referred to 100 g of the initial ES layer, and estimated by applying Peleg's model to the experimental data. Table 1 also includes the values of $1/k_1$ Peleg's parameter, related to the release rate. A good fit of the model was achieved in every case (R^2> 0.998), as can be seen in Figure 3. Both the release rate and asymptotic value were greatly affected by the polarity of the food simulants. The fastest release of CA was observed in 50% ethanol (D1 simulant) and isooctane (D2 simulant), whereas the slowest delivery occurred in the more polar solvents (A: 10% ethanol and B: 3% acetic acid). Those less polar solvents also allow for the maximum delivery of CA from the PCL mats (near 100% of their content), whereas only 75 and 57 % of the content was released at equilibrium in polar

342 solvents (simulants A and B, respectively). This behaviour agrees with the differences in
343 polarity of the solvent and the corresponding chemical affinity between the polymer matrix, the
344 active compound and the solvent, as previously reported by Tehrany (2007). In fact, three steps
345 can be described for the active release from the polymeric matrix: 1) solvent diffusion into the
346 polymer network, 2) network relaxation due to solvent plasticization effects, and 3) the
347 diffusion of the compound through the relaxed polymer network, until the thermodynamic
348 equilibrium between the polymer and food system phases is reached (Requena et al., 2017).
349 These steps can be coupled, especially 2 and 3, depending on the characteristic relaxation time
350 of polymers and the diffusion times of the diffusing compound, giving rise to anomalous
351 transport behaviour (Siepmann & Peppas, 2011). At equilibrium, the relative compound affinity
352 with the solvated polymer and its solubility in the liquid food system determine its partition
353 coefficient, defined as the ratio between the mass of active released at equilibrium in the
354 simulant (M_∞) and its corresponding residual mass in the film (M_0–M_∞). The solubility of CA
355 increases in less polar solvents with respect to the more aqueous solvents (CA water solubility is
356 1250 mg/L, Yalkowsky, He & Jain, 2010), while the PCL matrix could be more relaxed in
357 contact with non-polar solvents than with the more aqueous systems, considering the non-polar
358 nature of the polymer. Both the increase in the active solubility and polymer relaxation in less
359 polar food simulants led to a faster CA release and a higher amount of CA delivered at
360 equilibrium.

361 Table 1 also shows the parameters of the Korsmeyer and Peppas model. The values for the "n"
362 exponent reveal that a Fickian diffusion ($n \approx 0.5$) takes place when the matrix is in contact with
363 the less polar simulants, whereas an anomalous transport ($0.5<n<1.0$) can be assumed in the
364 aqueous media (Siepmann &Peppas, 2011), which reveals the coupling of the polymer
365 relaxation in contact with the solvent and the diffusion of CA in the matrix. This agrees with the
366 low solvent-polymer affinity, which will imply a poor capacity of the solvent to penetrate the
367 polymer network. Nevertheless, an apparent diffusion value (D) was estimated in every case
368 (Table 1) considering the electrospun layer thickness (0.16 ± 0.08 mm) and assuming a
369 homogenous medium, despite the nano-porous structure generated in the ES process (Figure 1),
370 where the solvent could also penetrate by means of capillarity. Figure 4 shows the curves fitted
371 considering the Fickian equation (eq. 1), where the good fit of the model can be appreciated,
372 (SSE < 0.12). The obtained D values also reflect the effect of the solvent polarity, showing the
373 highest values for simulant D (isooctane) and the lowest value for 10% ethanol in water
374 (simulant A). Other authors also report similar behaviour for the CA release from non-polar
375 polymer matrices, such as polypropylene (Ramos et al., 2014) and poly (butylene succinate)
376 (Petchwattana & Naknaen, 2015). Kuorwel, Cran, Sonneveld, Miltz & Bigger (2013) obtained
377 lower diffusion values (about 15 times lower) for the CA diffusion from starch films in
378 isooctane, which can be explained by the lower chemical affinity of starch matrix and isooctane,
379 which affects the polymer relaxation and plasticization level, and so, the compound diffusion.

From the obtained kinetic behaviour, no total CA release would be expected from PCL mats in the more polar food systems regardless of their pH, whereas it would be fully delivered in more fatty foods, due to the greater CA solubility and polymer relaxation during the food contact. Likewise, less time will be required for the maximum release in fatty foods (emulated by D1 and D2 simulants), than in more aqueous products (emulated by A and B simulants), where longer times would be needed.

3.3. Antibacterial properties of the CA loaded fibres

Based on the release profile, the amount of CA released in the incubation plates (55 mm in diameter, with 10 mL of agar medium), used in the *in vitro* antimicrobial test, was predicted, considering the behaviour of the medium to be similar to that of the simulant A (10 % ethanol in water). Figure 5 shows the predicted concentration of active reached over time for two CA-loaded PCL mats of different thicknesses (60 and 90 min of electrodeposition), and so, with different total amounts of CA in the mat. Likewise, the previously reported range for the MIC values of the tested foodborne bacteria, namely *E. coli* (0.225-5 $mg \cdot mL^{-1}$) and *L. monocytogenes* (0.375-5 $mg \cdot mL^{-1}$) (Burt, 2004) were reflected in the plot (shadow areas). The predicted equilibrium values for CA release for 60 and 90 min processed PCL mats greatly differed. In the case of the 60-min process, the MIC value for *E. coli* was barely reached, while the MIC value for *L. innocua* was higher than the amount of CA released. For the 90-min process, both MIC values were reached, but for *L. innocua*, the amount released at equilibrium was in the range limit after about 5 h of contact. This can imply a lack of antilisterial activity, since a high degree of bacterial growth will occur during this period.

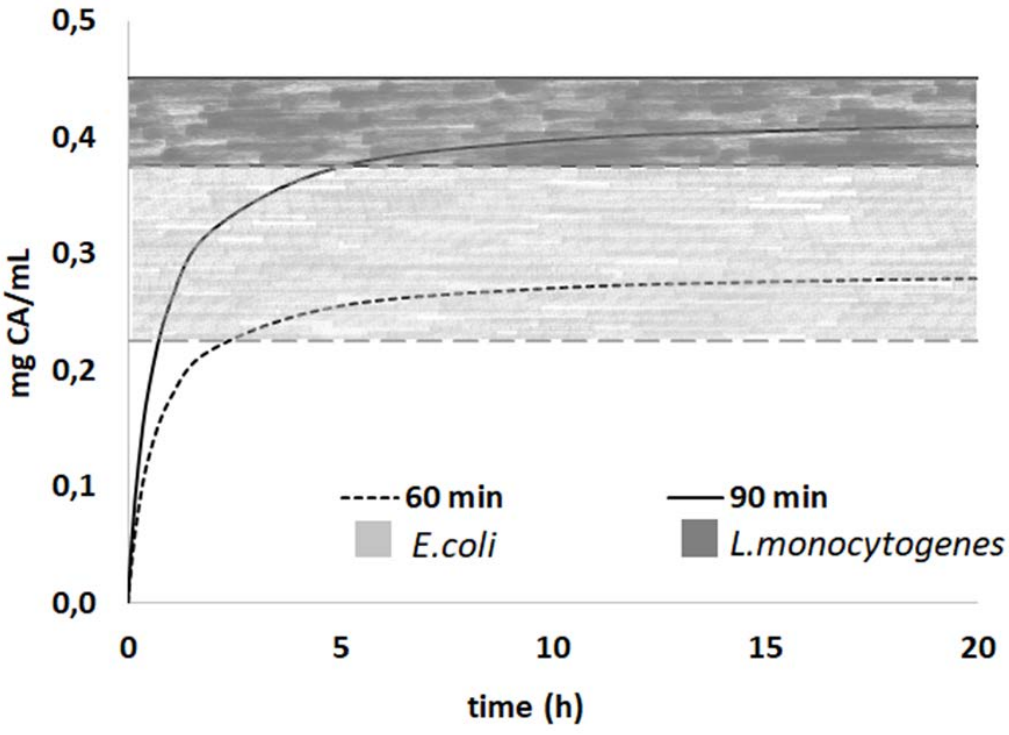

Figure 5. CA release prediction as a function of time in the microbial plate, assuming the behaviour of A simulant (10% ethanol). MIC range for *E. coli* is from $2.25 \cdot 10^{-4}$ g/mL (Cosentino et al., 1999) to $3.75 \cdot 10^{-4}$ g/mL (Du et al., 2015); MIC range for *L. monocytogenes* is from $3.75 \cdot 10^{-4}$ g/mL (Pol & Smid, 1999) to $4.5 \cdot 10^{-4}$g/mL (Cosentino et al., 1999)

Figure 6 shows the growth curves of both *E. coli* and *L. innocua* for 14 days, obtained in the *in vitro* test, for the control samples (uncoated and CA-free PCL coated) and for the samples coated with CA-loaded PCL mats electrodeposited for 60 and 90 min. No antilisterial effect was observed for either CA loaded PCL mat, according to the predicted CA release which did not reach or barely attained the MIC levels at longer contact times when the bacteria have grown to a great extent. Limitations in the CA release from PCL mat to aqueous systems compromise the antilisterial activity of the CA loaded mats, despite the enough CA load revealed by Figure 2b. For *E. coli*, a bacteriostatic effect was observed from 2 incubation days onwards, revealing that enough CA was released from the mat electrodeposited for 60 min at this contact time. For the 90-min electrodeposited mat, bacterial death progressively occurred from 2 days of contact onwards, when more CA release occurred in the culture medium. The obtained antimicrobial action of the CA-loaded PCL mats was coherent with the total load of CA, its release kinetics in the culture medium (assuming its behaviour as simulant A) and the MIC values of the respective bacteria. From this analysis, thicker CA-loaded PCL mats, with a greater surface density of CA, would be required to obtain antilisterial activity, whereas 90-min electrodeposited mats were able to exert an antibacterial effect against E. coli, taking into account the total CA load and its release kinetics in the culture medium.

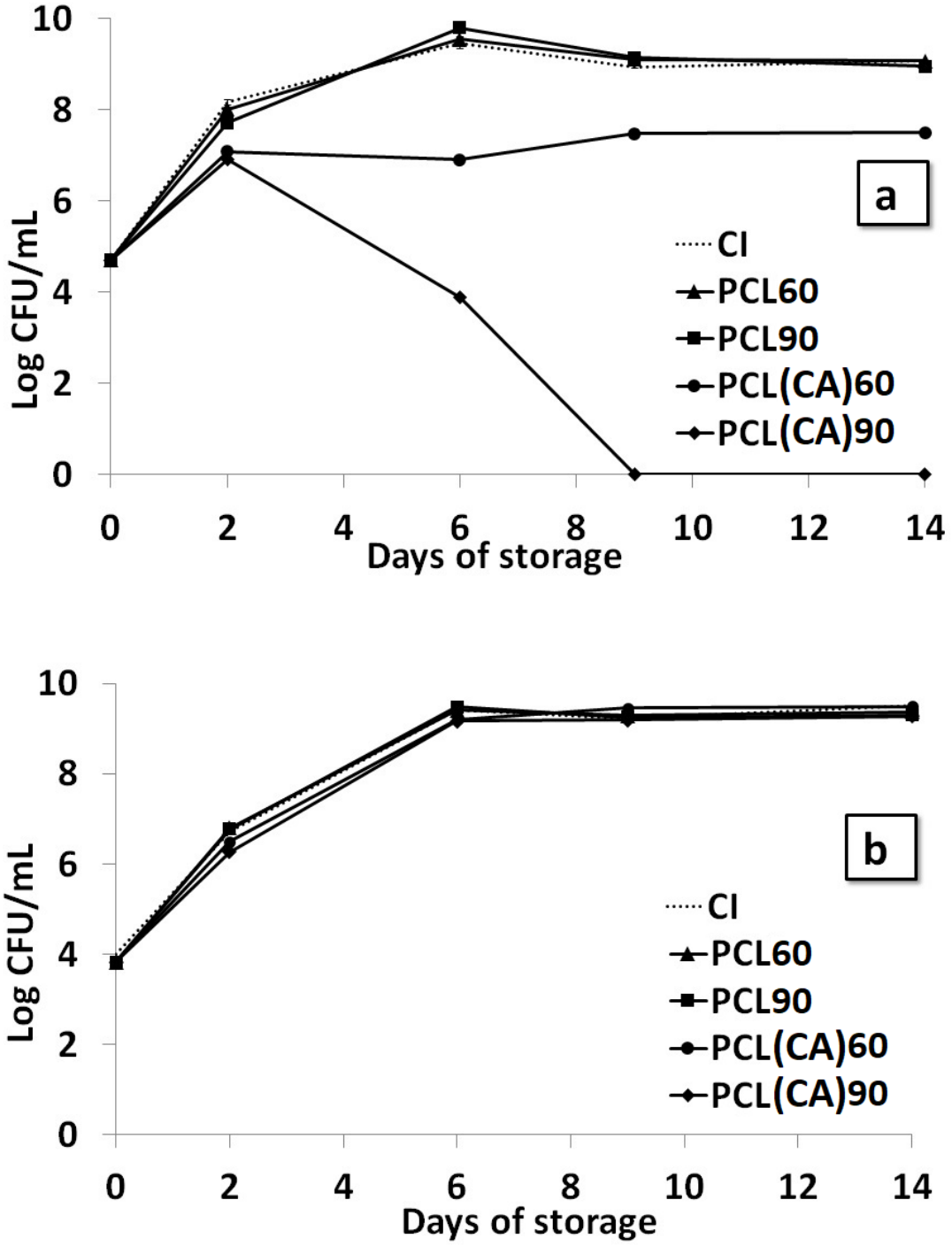

Figure 6. Growth of *E. coli* (**a**) and *L. innocua* (**b**) in the culture media at 10 ºC in the uncoated inoculum control plate (CI) and plates coated with electrospun PCL without CA (PCL60; PCL90) and with electrospun PCL with CA (PCL(CA)60; PCL(CA)90). The numbers 60 and 90 indicate the electrodeposition time of fibres.

3.4 Multilayer starch films with electrospun PLC fibres with and without CA

The efficiency with which PCL electrospun fibres improve the functional properties of starch films, either as packaging material or antimicrobial activity, was analysed through the measurement of the tensile, barrier and optical properties of the films as well as the *in vitro*

antibacterial capacity for *E. coli* and *L. innocua*. Table 2 shows the different film properties, where the effect of the electrospun PCL layer between the two starch sheets can be observed.

Table 2. Barrier (water vapour permeability: WVP and Oxygen permeability: OP), tensile (Elastic modulus: EM, tensile strength: TS and deformation at break: %ε) and optical properties (Internal transmittance: Ti, Gloss (60º), lightness: L*, chrome: C_{ab} and hue: h_{ab}) of starch multilayer films containing electrospun PCL fibres. Different superscript letters in the same row indicate significant differences ($p<0.05$) between multilayers.

	Multilayer				
	S-S	**S-PCL60-S**	**S-PCL(CA)60-S**	**S-PCL90-S**	**S-PCL(CA)90-S**
Thickness [mm]	0.38 ± 0.07^{a}	0.45 ± 0.01^{b}	0.45 ± 0.01^{b}	0.44 ± 0.03^{b}	0.5 ± 0.02^{b}
WVP[g/(Pa·s·m)]	570 ± 40^{c}	180 ± 60^{b}	190 ± 40^{b}	120 ± 20^{a}	94 ± 10^{a}
OP x 10^{14} [cm^3/ Pa·s·m]	5 ± 3^{a}	3.6 ± 0.4^{a}	5 ± 1^{a}	4 ± 2^{a}	2.9 ± 0.6^{a}
EM [MPa]	206 ± 21^{b}	149 ± 23^{a}	126 ± 34^{a}	192 ± 32^{b}	126 ± 23^{a}
TS [MPa]	9.7 ± 0.7^{d}	7 ± 2^{bc}	6.2 ± 0.9^{ab}	8 ± 1^{c}	5.8 ± 0.8^{a}
%ε	39 ± 4^{b}	34 ± 15^{ab}	34 ± 10^{ab}	36 ± 5^{ab}	29 ± 6^{a}
T_i [460 nm]	0.73 ± 0.01^{c}	0.72 ± 0.01^{bc}	0.69 ± 0.01^{ab}	0.69 ± 0.04^{ab}	0.69 ± 0.02^{a}
Gloss [60º]	15 ± 2^{b}	17 ± 4^{b}	9 ± 2^{a}	18 ± 5^{b}	10 ± 3^{a}
L*	65.7 ± 0.6^{b}	64.8 ± 0.9^{ab}	64.6 ± 0.8^{ab}	66 ± 2^{b}	64.2 ± 0.4^{a}
C_{ab}	21.3 ± 0.3^{ab}	21.2 ± 0.3^{ab}	21.0 ± 0.6^{ab}	21 ± 1^{a}	21.7 ± 0.3^{b}
h_{ab}	79.8 ± 0.4^{c}	79.4 ± 0.4^{bc}	78.9 ± 0.6^{ab}	79.5 ± 0.5^{c}	78.7 ± 0.2^{a}

The ES layer thickness in the multilayer film can be deduced from the respective difference values as regards the SS bilayer. The resulting thickness was affected not only by the ES layer thickness but also by the relative radial flow of the PCL in the mats during the thermocompression step of multilayer. In general, no significant differences were observed in the measured thicknesses of the multilayer films, all of which were about 70-120 μm thicker than the SS bilayer. This indicates that, regardless of the initial thickness of the ES layer, its flow and compaction during thermocompression led to non-significant differences in the multilayer film thicknesses. The equilibrium moisture content of the multilayers was not significantly affected by the presence of the PCL fibre, this being 7.3 ± 0.2 g/100 g dry film.

As concerns the barrier properties, the WVP was greatly reduced when PCL fibres were present between the starch layers: 65 and 80 % reductions for 60 and 90-min electrodeposited layers, respectively **(**Table 2**).** This indicates the effectiveness of the parallel assembly of the PCL sheet, with a different surface density in the multilayer film, at limiting the transport of water molecules, as previously observed in starch-PCL bilayer films by Ortega-Toro et al. (2015). Nevertheless, no changes in the oxygen permeability of the SS films were observed, due to the fact that starch layers are actually the limiting material for the gas transport. As concerns tensile behaviour, the inclusion of PCL mats in multilayer films implied a slight reduction of the film stiffness and tensile at break, which can be attributed to the discontinuity introduced at the interlayer zone in the multilayer. This reduced the film's cohesion forces at the interfacial area, where no great chemical affinity could be expected for the PCL chains in contact with the starch matrix. However, no significant changes in the film extensibility were observed, except when CA-loaded PCL fibre produced for 90 min was included. In this case, films become slightly less stretchable and resistant, which could be attributed to a certain degree of CA diffusion into the starch matrix of bilayer, giving rise to a weakening effect in the starch multilayer. This effect

was also observed at lower intensity in multilayers containing 60 min electrospun PCL with CA. The optical properties of the multilayer films were hardly affected by the PCL mat inclusion. The internal transparency (T_i) was the most affected optical property due to the greater opacity of PCL than starch (Ortega-Toro et al., 2015).

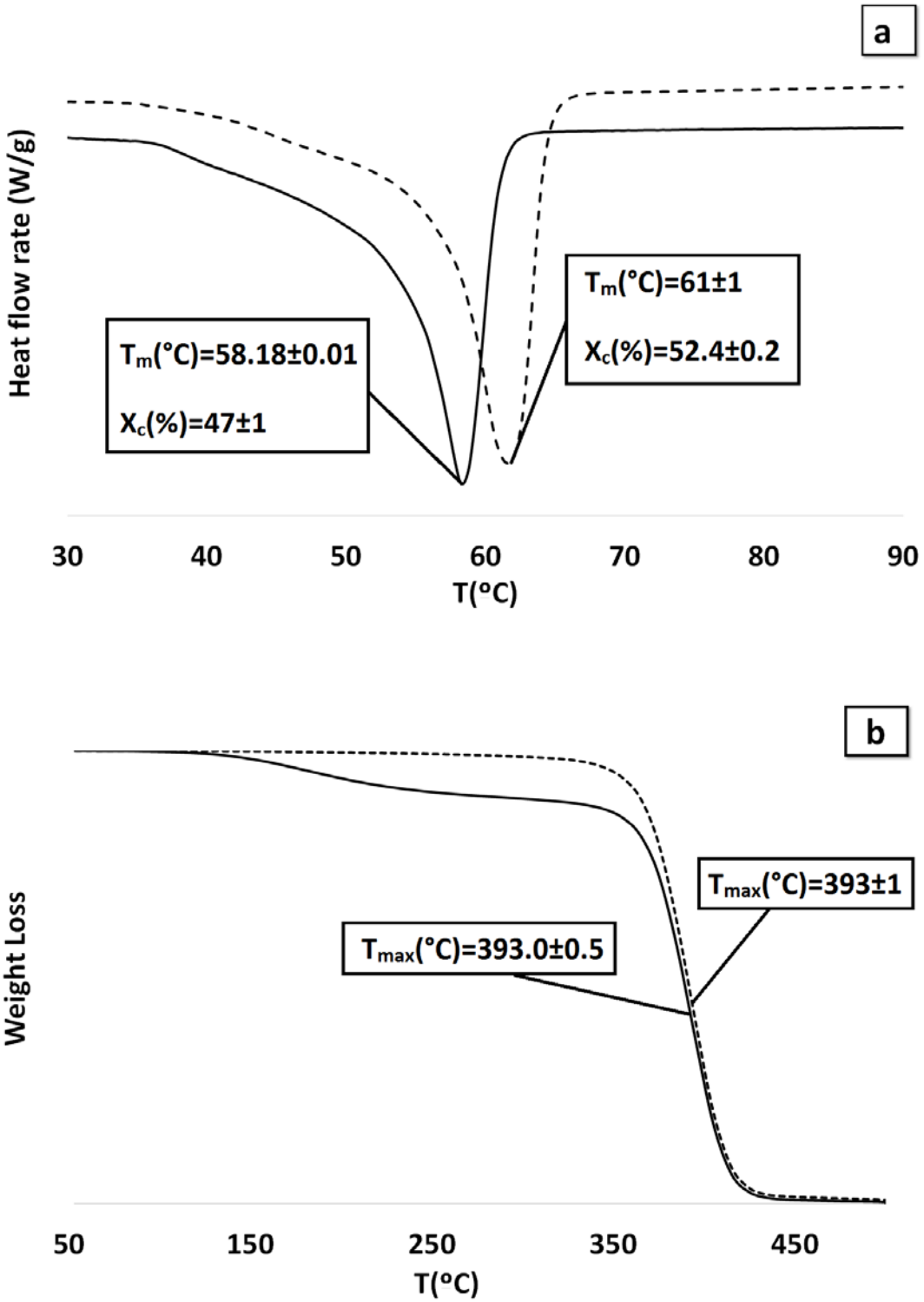

Figure 7. a) DSC thermograms and **b**) TGA curves of electrospun PCL fibres carrying (continuous line) or not (dashed line) CA. Melting temperature (T_m) and crystallization degree (X_c) as well as temperature for the maximum degradation rate (T_{max}) of PCL are shown for each sample.

DSC and TGA analyses of isolated PCL fibres and multilayers were carried out to identify changes in phase transitions or thermal stability of the polymers, either starch or PCL, associated with the presence of CA or with its internal diffusion in the multilayer. Figures 7a and b show the DSC thermograms (first heating step) for both fibres as well as the TGA curves. The melting endotherm of PCL can be observed for both mats, showing a shift of the melting peak to lower temperatures when fibres contained CA. From the melting enthalpy and the mass of PCL in each sample, the crystallization degree of PCL was estimated, by considering the enthalpy value of completely crystallized PCL (139.3 J/g, as reported by Koenig & Huang, 1995). A decrease in the PCL crystallization degree was also observed in CA-loaded fibres. These results point to the effective miscibility of CA and PCL in the fibres, which reduced the melting point and crystallinity of the polymer, as previously reported for CA containing PHBV (Requena, Jiménez, Vargas & Chiralt, 2016). TGA curves (Figure 7b) show the influence of the CA-load on the thermal behaviour of the mats. Weight losses at temperatures below the PCL thermodegradation must be attributed to the CA evaporation from the mat, which did not affect the temperature of the maximum degradation rate (393.2 ± 0.6ºC) of the polymer, but overlapped the starting degradation step.

In contrast, DSC thermograms of multilayer films also revealed the crystalline structure of PCL in the electrospun layer, although no effect of CA was observed on its crystallization and melting temperatures (Table 3), which coincided with those observed for pure PCL mats, these being in the range previously reported for PCL films (Ortega-Toro et al., 2015). The values of crystallization and melting enthalpy from the different scans did not show significant differences for a determined sample, which indicates that the film process formation induced similar PCL crystallization to that obtained in the DSC scan conditions. Small differences in the enthalpy values among the different samples can be attributed to the fluctuations in the electrospun layer thickness in the different small bilayer samples used in the DSC analysis. This melting behaviour of PCL in multilayers, similar to that of pure PCL fibres, suggests that a high proportion of CA migrated to the starch sheets in the multilayer assembly, since the potential remaining amount in the PCL internal sheet was not enough to affect the PCL melting behaviour. On the other hand, the glass transition temperature of the starch (Table 3) was slightly reduced in multilayers containing CA-loaded fibres, particularly when this fibre mat was thicker, with the subsequent higher load of CA. This is coherent with the afore-mentioned small changes in the tensile behaviour of multilayers containing carvacrol.

Table 3. Phase transitions in the starch multilayer films containing electrospun PCL fibres (glass transition temperature of starch (T_g), and melting and crystallization temperatures and enthalpy of PCL). Different superscript letters in the same row indicate significant differences ($p<0.05$) between multilayers.

		Multilayer				
		S-S	**S-PCL60-S**	**S-PCL(CA)60-S**	**S-PCL90-S**	**S-PCL(CA)90-S**
T_g (midpoint)	**1st scan**	107 ± 3^{ab}	$108{,}0 \pm 0{,}6^{ab}$	108 ± 8^{b}	101 ± 2^{ab}	98 ± 4^{a}
1st heating	**ΔH_m (J/g)**	-	1.36 ± 0.12^{a}	3.45 ± 0.04^{b}	1.9 ± 0.2^{a}	3.8 ± 0.5^{b}

step	**T_m (peak)**	-	62.7 ± 0.5^{b}	62.8 ± 0.6^{b}	60.9 ± 0.4^{a}	61.6 ± 0.4^{a}
2nd heating step	**ΔH_m (J/g)**	-	0.90 ± 0.04^{a}	2.5 ± 0.2^{bc}	1.5 ± 0.2^{ab}	3 ± 1^{c}
	T_m (peak)	-	55.79 ± 0.09^{a}	55.6 ± 0.5^{a}	55.9 ± 0.2^{a}	56.6 ± 0.4^{b}
Cooling step	**ΔH_c (J/g)**	-	1.20 ± 0.04^{a}	3.1 ± 0.2^{b}	1.9 ± 0.7^{a}	3.6 ± 0.8^{b}
	T_c	-	29 ± 1^{a}	28.4 ± 0.9^{a}	28.5 ± 0.6^{a}	27.5 ± 0.4^{a}

Likewise, the thermal degradation (Figure 8 a and b) of multilayer films exhibited the two typical steps associated with starch and PCL degradation, where the influence of CA can also be observed. Weight loss started earlier in 60-min electrospun CA-loaded fibres (from about 130ºC), associated with the CA evaporation, but had no significant effect on the temperature of maximum degradation rate of starch. Nevertheless, in 90-min electrospun fibres, with a greater CA load, a shifting of this temperature occurred which indicated the CA-starch interactions as a result of the CA diffusion into the starch layers. On the other hand, the thermodegradation of PCL was also affected by CA interactions, exhibiting a lower temperature in the maximum degradation rate. A higher residual mass was also observed in CA-loaded multilayers. This behaviour suggests the participation of CA in both starch and PCL matrices with enough interaction forces to modify their thermal stability and modify the tensile behaviour of the films, as previously commented.

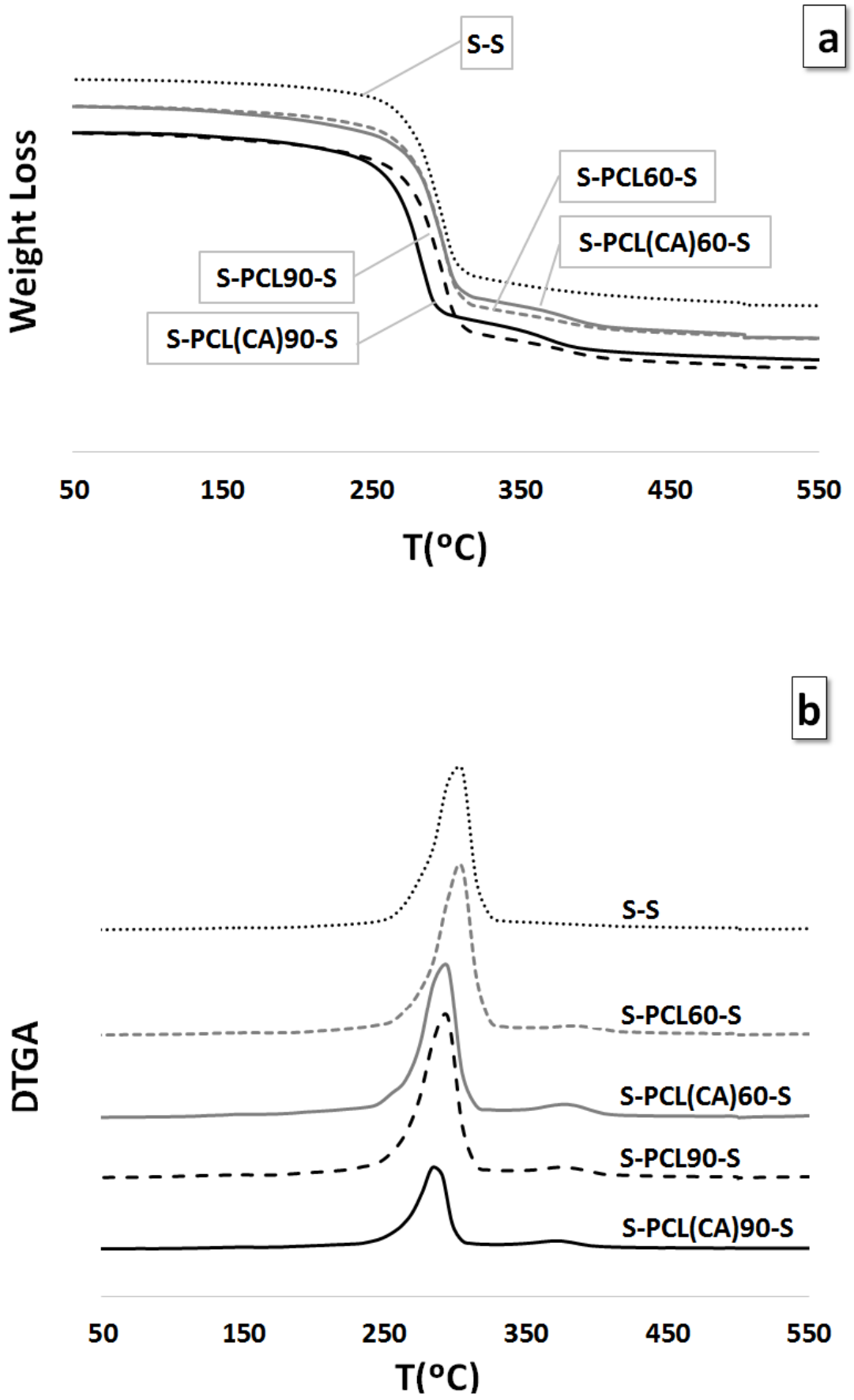

Figure 8. TGA (**a**) and DGTA(**b**) curves of starch multilayer films containing 60 (grey) or 90 (black) min electrospun PCL fibres, with (continuous line) and without (dashed line) CA.

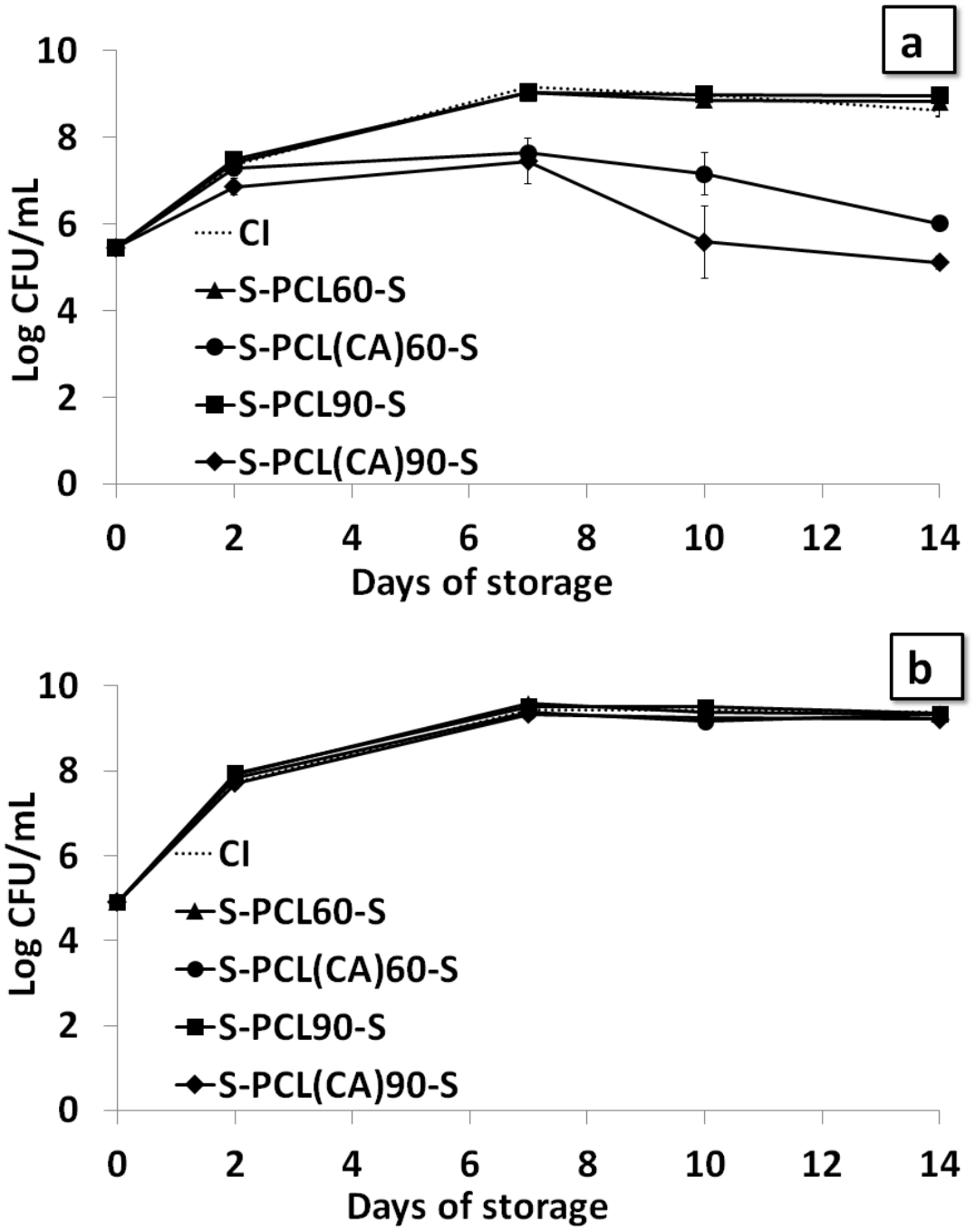

Figure 9. Growth of *E. coli* (**a**) and *L. innocua* (**b**) in the culture media at 10ºC in the inoculum plates, coated with starch multilayers with 60 or 90 min electrospun CA loaded layers (S-PCL(CA)60-S and S-PCL(CA)90-S). Controls: uncoated inoculated plates (CI) and those coated with CA-free multilayers (S-PCL60-S and S-PCL90-S).

The CA diffusion into the starch layers could affect the antimicrobial activity of the multilayer films, with respect to that observed for CA-loaded mats, which was analysed. The antibacterial activity of the multilayer films revealed from the *in vitro* test (Figure 9), indicates a similar behaviour to that observed for the CA-loaded PCL mats. No antilisterial effect was observed, while a delayed action against E. coli was observed. This delay can be explained by the thicker layer (starch layer) where CA must diffuse to reach the target point in the culture medium. From 2 to 7 contact days, a bacteriostatic effect could be appreciated; from 7 contact days onwards, however, a bactericidal action was observed both for 60 and 90-min CA-loaded electrospun PC.

This effect was more intense when CA-loaded fibres were thicker (90 min electrodeposited), in agreement with the higher CA load in the multilayer. Then, CA-loaded electrospun PCL fibres applied to multilayer starch films allows for effective antibacterial action against *E. coli* to a similar extent to that observed in the isolated fibres, but with a slightly retarded effect. Likewise, the electrospun PCL layers were greatly effective at reducing the WVP values of starch films, without relevant changes in their tensile or optical properties.

Conclusions

Electrospun PCL fibre mats encapsulating CA were effective at controlling the growth of *E. coli*, when the surface density of CA loaded fibres was 1.2 and 1.8 mg/cm^2, the latter being more effective. In both cases, the CA released into the culture medium exceeded the MIC of the bacteria. Nevertheless, these mats were not effective at controlling the growth of *L. innocua*, since a greater release of CA was necessary to achieve the MIC of this bacterium. Not only did the CA load in the fibres determine their antimicrobial effect, but also its release capacity into the aqueous media. In this sense, the fibre showed a faster release and higher release capacity of the active in fatty foodstuffs (simulants D1 and D2), where practically the total amount of CA could be released from the fibres. However, in more aqueous food systems (simulants A and B), such as the bacteria culture medium, a more limited CA delivery (60-75 %) occurred with a slower rate, which reduced the potential effectiveness of the encapsulated active. This meant that the Gram negative bacteria (*E. coli*) could be effectively inhibited, whereas no growth inhibition was observed for Gram positive (*L. innocua*), which would require a greater surface density of the electrospun CA-loaded PCL fibres. This behaviour was reproduced in multilayer starch films containing the CA-loaded electrospun PCL fibres between two starch sheets, although a delayed response was observed for the antimicrobial action. In these multilayer films, a great reduction in the water vapour permeability was also observed with respect to that of starch films, without any notable changes in the other packaging functions. Therefore, active electrospun PCL fibre in multilayer starch films represents an interesting alternative for the purposes of active food packaging.

Acknowledgements

The authors thank the Ministerio de Economia y Competitividad (MINECO) of Spain, for the financial support for this study as a part of projects AGL2013-42989-R and AGL2016-76699-R. The author A. Tampau thanks MINECO for the pre-doctoral research grant # BES-2014-068100.

References

1.ASTM. (1995). Standard test methods for water vapor transmission of materials. standard designations: E96-95. In ASTM, annual book of ASTM (pp. 406-413). Philadelphia, PA: American Society for Testingand Materials.

2.ASTM. (2001). Standard test method for tensile properties of thin plastic sheeting. Standard Designations: D882. In Annual book of ASTM standards (pp 162-170). Philadelphia, PA: American Society for Testing and Materials.

3.ASTM. (2002). Standard test method for oxygen gas transmission rate through plastic film and sheeting using a coulometric sensor. Standard Designations: 3985-95.In Annual book of ASTM standards (pp 472-477). Philadelphia, PA: American Society for Testingand Materials.

4.Bahrami, S. H., & Gholipour Kanani, A. (2011). Effect of changing solvents on poly(ε-Caprolactone) nanofibrous webs morphology. *Journal of Nanomaterials*, *2011*. https://doi.org/10.1155/2011/724153

5.Ben Arfa, A., Combes, S., Preziosi-Belloy, L., Gontard, N., & Chalier, P. (2006). Antimicrobial activity of carvacrol related to its chemical structure. *Letters in Applied Microbiology*, *43*(2), 149–154. https://doi.org/10.1111/j.1472-765X.2006.01938.x

6.Bhardwaj, N., & Kundu, S. C. (2010). Electrospinning: A fascinating fiber fabrication technique. *Biotechnology Advances*, *28*(3), 325–347. https://doi.org/10.1016/j.biotechadv.2010.01.004

7.Burt, S (2004). Essential oils: their antibacterial properties and potential applications in foods—a review. International Journal of Food Microbiology 94 (3) 223– 253 http://dx.doi.org/10.1016/j.ijfoodmicro.2004.03.022

8.Commission, E. (2011). EU Guidance to the Commission Regulation (EC) No 450 / 2009 of 29 May 2009 on active and intelligent materials and articles intended to come into contact with food., (450), 1–26.

9.Cosentino, S., Tuberoso, C. I. G., Pisano, B., Satta, M., Mascia, V., Arzedi, E., & Palmas, F. (1999). In-vitro antimicrobial activity and chemical composition of Sardinian Thymus essential oils. *Letters in Applied Microbiology*, *29*(2), 130–135. https://doi.org/10.1046/j.1472-765X.1999.00605.x

10.Crank, J. (1979). *The Mathematics of Diffusion*, (2nd ed.) London: Oxford University Press, (Chapter 4).

11.Du, E., Gan, L., Li, Z., Wang, W., Liu, D., & Guo, Y. (2015). In vitro antibacterial activity of thymol and carvacrol and their effects on broiler chickens challenged with Clostridium perfringens. *Journal of Animal Science and Biotechnology*, *6*(1), 58. https://doi.org/10.1186/s40104-015-0055-7

12.Efsa. (2012). Scientific Opinion on the Safety and efficacy of phenol derivates containing ring-alkyl, ring-alkoxy and side- chains with an oxygenated functional group (chemical group 25) when used as flavourings for all species. *Efsa J.*, *10*(2), 2573. https://doi.org/10.2903/j.efsa.2012.2573.

615 13.Fabra, M. J., López-Rubio, A., & Lagaron, J. M. (2016). Use of the electrohydrodynamic
616 process to develop active/bioactive bilayer films for food packaging applications. *Food*
617 *Hydrocolloids*, *55*, 11–18. https://doi.org/10.1016/j.foodhyd.2015.10.026

618 14.Fernández-Pan, I., Maté, J. I., Gardrat, C., & Coma, V. (2015). Effect of chitosan molecular
619 weight on the antimicrobial activity and release rate of carvacrol-enriched films. *Food*
620 *Hydrocolloids*, *51*, 60–68. https://doi.org/10.1016/j.foodhyd.2015.04.033

621 15.Fu, Y., Sarkar, P., Bhunia, A. K., & Yao, Y. (2016). Delivery systems of antimicrobial
622 compounds to food. *Trends in Food Science and Technology*, *57*, 165–177.
623 https://doi.org/10.1016/j.tifs.2016.09.013

624 16.Gennadios A., Weller C. L, & Gooding C. H. (1994). Measurement errors in water vapor
625 permeability of highly permeable, hydrophilic edible films. Journal of Food Engineering,
626 Volume 21, Issue 4, pp 395-409, ISSN 0260-8774. https://doi.org/10.1016/0260-
627 8774(94)90062-0.

628 17.Hamori, M., Yoshimatsu, S., Hukuchi, Y., Shimizu, Y., Fukushima, K., Sugioka, N.,
629 Nishimura, A., & Shibata, N. (2014). Preparation and pharmaceutical evaluation of nano-
630 fiber matrix supported drug delivery system using the solvent-based electrospinning
631 method. *International Journal of Pharmaceutics*, *464*(1–2), 243–251.
632 https://doi.org/10.1016/j.ijpharm.2013.12.036

633 18.Hernández-Martínez, D., Nicho, M. E., Hu, H., León-Silva, U., Arenas-Arrocena, M. C., &
634 García-Escobar, C. H. (2017). Electrospinning of P3HT-PEO-CdS fibers by solution
635 method and their properties. *Materials Science in Semiconductor Processing*, *61*
636 (November 2016), 50–56. https://doi.org/10.1016/j.mssp.2016.12.039

637 19.Higueras, L., López-Carballo, G., Hernández-Muñoz, P., Catalá, R., & Gavara, R. (2014).
638 Antimicrobial packaging of chicken fillets based on the release of carvacrol from
639 chitosan/cyclodextrin films. *International Journal of Food Microbiology*, *188*, 53–59.
640 https://doi.org/10.1016/j.ijfoodmicro.2014.07.018

641 20.Hines, D. J., & Kaplan, D. L. (2012). Mechanims of controlled release from silk fibroin
642 films. *Changes*, *29*(6), 997–1003.
643 https://doi.org/10.1016/j.biotechadv.2011.08.021.Secreted

644 21.Joint FAO/WHO, June 2001. Expert Committee on Food Additives Fifty-fifth report.
645 http://apps.who.int/iris/bitstream/10665/42388/1/WHO_TRS_901.pdf (accessed on August
646 04, 2017).

647 22.Koenig, M. F., & Huang, S. J. (1995). Biodegradable blends and composites of
648 polycaprolactone and starch derivatives. *Polymer*, *36*(9), 1877–1882.

649 23.Kuorwel, K. K., Cran, M. J., Sonneveld, K., Miltz, J., & Bigger, S. W. (2013). Migration of
650 antimicrobial agents from starch-based films into a food simulant. *LWT - Food Science*
651 *and Technology*, *50*(2), 432–438. https://doi.org/10.1016/j.lwt.2012.08.023

652 24.López, O. V., Zaritzky, N. E., Grossmann, M. V. E., & García, M. A. (2013). Acetylated and
653 native corn starch blend films produced by blown extrusion. *Journal of Food Engineering*,
654 *116*(2), 286–297. https://doi.org/10.1016/j.jfoodeng.2012.12.032

655 25.Macagnano, A., & De Cesare, F. (2017). 17 - Electrospinning: A versatile technology to
656 design biosensors and sensors for diagnostics. In E. B. T.-E. M. for T. E. and B. A. Kny
657 (Ed.) (pp. 385–417). Woodhead Publishing. https://doi.org/10.1016/B978-0-08-101022-
658 8.00016-8

659 26.Majid, I., Ahmad Nayik, G., Mohammad Dar, S., & Nanda, V. (2016). Novel food packaging
660 technologies: Innovations and future prospective. *Journal of the Saudi Society of*
661 *Agricultural Sciences*. https://doi.org/10.1016/j.jssas.2016.11.003

662 27.Mercante, L. A., Scagion, V. P., Migliorini, F. L., Mattoso, L. H. C., & Correa, D. S. (2017).
663 Electrospinning-based (bio)sensors for food and agricultural applications: A review. *TrAC*
664 *- Trends in Analytical Chemistry*, *91*, 91–103. https://doi.org/10.1016/j.trac.2017.04.004

665 28.Ortega-Toro, R., Morey, I., Talens, P., & Chiralt, A. (2015). Active bilayer films of
666 thermoplastic starch and polycaprolactone obtained by compression molding.
667 *Carbohydrate Polymers*, *127*, 282–290. https://doi.org/10.1016/j.carbpol.2015.03.080

668 29.Padgett, T., Han, I. Y., & Dawson, P. L. (1998). Incorporation of food-grade antimicrobial
669 compounds into biodegradable packaging films. *Journal of Food Protection*, *61*(10),
670 1330–1335.

671 30.Peleg, M. (1988). An Empirical Model for the Description Moisture Sorption Curves.
672 *Journal of Food Science*, *53*(4), 1216–1217. https://doi.org/10.1111/j.1365-
673 2621.1988.tb13565.x

674 31.Perdones, Á., Chiralt, A., & Vargas, M. (2016). Properties of film-forming dispersions and
675 films based on chitosan containing basil or thyme essential oil. *Food Hydrocolloids*, *57*,
676 271–279. https://doi.org/10.1016/j.foodhyd.2016.02.006

677 32.Petchwattana, N., & Naknaen, P. (2015). Utilization of thymol as an antimicrobial agent for
678 biodegradable poly (butylene succinate). *Materials Chemistry and Physics*, *163*, 369–375.
679 https://doi.org/10.1016/j.matchemphys.2015.07.052

680 33.Pol, I. E., & Smid, E. J. (1999). Combined action of nisin and carvacrol on Bacillus cereus
681 and Listeria monocytogenes. *Letters in Applied Microbiology*, *29*(3), 166–170.
682 https://doi.org/10.1046/j.1365-2672.1999.00606.x

683 34.Pushpadass[a], H. A., Kumar[a], A., Jackson[b], D. S., Wehling[b], R. L., Dumais[c], J. J., &
684 Hannaa, M. A. (2009). Macromolecular changes in extruded starch-films plasticized with
685 glycerol, water and stearic acid. *Starch/Staerke*, *61*(5), 256–266.
686 https://doi.org/10.1002/star.200800046

687 35.Ramos, M., Beltrán, A., Peltzer, M., Valente, A. J. M., & Garrigós, M. del C. (2014).
688 Release and antioxidant activity of carvacrol and thymol from polypropylene active
689 packaging films. *LWT - Food Science and Technology*, *58*(2), 470–477.
690 https://doi.org/10.1016/j.lwt.2014.04.019

691 36.Requena, R., Jiménez, A., Vargas, M., & Chiralt, A. (2016). Poly[(3-hydroxybutyrate)-co-(3-
692 hydroxyvalerate)] active bilayer films obtained by compression moulding and applying
693 essential oils at the interface. *Polymer International*, *65*(8), 883–891.
694 https://doi.org/10.1002/pi.5091

695 37.Requena, R., Vargas, M., & Chiralt, A. (2017). Release kinetics of carvacrol and eugenol
696 from poly(hydroxybutyrate-co-hydroxyvalerate) (PHBV) films for food packaging
697 applications. *European Polymer Journal*, *92*(May), 185–193.
698 https://doi.org/10.1016/j.eurpolymj.2017.05.008

699 38.Rieger, K. A., & Schiffman, J. D. (2014). Electrospinning an essential oil: Cinnamaldehyde
700 enhances the antimicrobial efficacy of chitosan/poly (ethylene oxide) nanofibers.
701 *Carbohydrate Polymers*, *113*, 561–568. https://doi.org/10.1016/j.carbpol.2014.06.075

702 39.Siepmann, J., & Peppas, N. A. (2011). Higuchi equation: Derivation, applications, use and
703 misuse. *International Journal of Pharmaceutics*, *418*(1), 6–12.
704 https://doi.org/10.1016/j.ijpharm.2011.03.051

705 40.Sill, T. J., & von Recum, H. A. (2008). Electrospinning: Applications in drug delivery and
706 tissue engineering. *Biomaterials*, *29*(13), 1989–2006.
707 https://doi.org/10.1016/j.biomaterials.2008.01.011

708 41.Tampau, A., González-Martinez, C., & Chiralt, A. (2017). Carvacrol encapsulation in starch
709 or PCL based matrices by electrospinning. *Journal of Food Engineering*, *214*, 245–256.
710 https://doi.org/10.1016/j.jfoodeng.2017.07.005

711 42.Tehrany, E. A., & Desobry, S. (2007). Partition coefficient of migrants in food
712 simulants/polymers systems. *Food Chemistry*, *101*(4), 1714–1718.
713 https://doi.org/10.1016/j.foodchem.2006.03.058

714 43.Tunc, S., Chollet, E., Chalier, P., Preziosi-Belloy, L., & Gontard, N. (2007). Combined effect
715 of volatile antimicrobial agents on the growth of Penicillium notatum. *International*
716 *Journal of Food Microbiology*, *113*(3), 263–270.
717 https://doi.org/10.1016/j.ijfoodmicro.2006.07.004

718 44.Ultee, A., Gorris, L. G. M., & Smid, E. J. (1998). Bactericidal activity of carvacrol towards
719 the food-borne pathogen Bacillus cereus. *Journal of Applied Microbiology*, *85*(2), 211–
720 218. https://doi.org/10.1046/j.1365-2672.1998.00467.x

721 45.Valencia-Sullca, C., Jiménez, M., Jiménez, A., Atarés, L., Vargas, M., & Chiralt, A. (2016).
722 Influence of liposome encapsulated essential oils on properties of chitosan films. *Polymer*
723 *International*, *65*(8), 979–987. https://doi.org/10.1002/pi.5143

724 46.Yalkowsky, S.H., He, Y., & Jain, P. (2010). Handbook of Aqueous Solubility Data (second
725 ed.) (pp 710). Florida, CRC Press.

726 47.Xue, J., Song, J., Dong, Y., Xu, L., Li, J., & Zeng, H. (2017). Nanowire-based transparent
727 conductors for flexible electronics and optoelectronics. *Science Bulletin*, *62*(2), 143–156.
728 https://doi.org/10.1016/j.scib.2016.11.009